

# MONTE CARLO OPTIMIZATION OF FAST BEAM LOSS MONITORS FOR LCLS-II\*

M. Santana Leitner<sup>†</sup>, C. I. Clarke, A. S. Fisher,  
A.M. Harris, C. Hast, SLAC National Accelerator Laboratory, Menlo Park, USA  
T. Liang, Deutsches Elektronen-Synchrotron, Hamburg, Germany  
E. Griesmayer, CIVIDEC Instrumentation, Vienna, Austria

## Abstract

Commissioning of the LCLS-II hard X-ray FEL at SLAC National Accelerator Laboratory has started. This facility and its successors will ultimately accelerate electrons to 8 GeV, with beams of 375 kW at 1 MHz. Potential errant beams of such high-powers, will need to be detected very fast -200  $\mu$ s- to limit exposure and to protect beam-line and safety components. Currently, the parent low-repetition-rate (LCLS) uses ion chamber technology, both as Point Beam Loss Monitors (PBLM) by collimators, dumps, septa, etc., and also as Long Beam Loss Monitors (LBLM) that provide detection coverage in extended areas where the accelerator enclosure is not sufficiently thick to shield full beam losses.

Due to the finite ion mobility and related screening effects, ion chambers are not fast enough for MHz beams, and their response would not be linear at high charge rates [1]. Consequently, LCLS-II has been designed with synthetic mono-crystalline diamond chips as PBLMs, which offer nanosecond time resolution due to the high mobility of holes in the valence band. LBLMs will be  $\approx$ 200 m-long optical fibers, with photomultipliers (PMT) that detect Čerenkov photons produced by charged particles interacting with the fibers. Models for these technologies were developed as scoring functions for the FLUKA Monte Carlo code [2, 3], and then were benchmarked and tuned against in-house experiments. Those models were then used to understand optimized placement of detectors considering shared use of detectors, response intensity or even radiation damage.

The limited scope of this paper just allows highlighting the basics of each of the processes and their subsequent conclusions.

## SYNTHETIC DIAMOND DETECTOR RESPONSE

All simulations and tests on diamond detectors described here refer to synthetic mono-crystalline diamond ( $C_{\{d\}}$ ) by CIVIDEC, named 'B1' type.

### Diamond Response Implementation

By using GEANT-4 [4], CIVIDEC simulated  $e^-$ /hole pair generation (i.e. charge in fC) in 500  $\mu$ m of  $C_{\{d\}}$  per interaction of photons, protons, neutrons, electrons or positrons of up to 1 GeV, as well as the total interaction rates by those

particles. The resulting data points for pair generation per interaction, and for total interaction probabilities, were then fitted to 5<sup>th</sup> degree polynomials, mostly on the Log-Log scale. Eventually, local function fitting to some energy ranges was also used.

The five sets of polynomials were programmed in the FLUKA user modifiable routine "fluscw.f", so that fluence scoring in every voxel of the geometry can be automatically weighted by the product of the interaction probability in  $C_{\{d\}}$  for the given particle at its current energy and its associated charge generation rate per interaction. Finally, in order to obtain the total signal fC per simulated primary, results should be multiplied by the actual detector volume (i.e.  $8 \times 10^{-3}$  cm<sup>3</sup> for B1) and divided by the  $500 \times 10^{-4}$  cm path. It should be noted that the detector signal is independent of its orientation. Actually, this implementation allows anticipating the diamond detector response field in space, not requiring to code the detector geometry (materials, etc.) at any precise location. Thus, a single setup allows assessing the response of diamonds located anywhere through the scoring volume.

### B1 Model Benchmarking and QA Process

Performance of B1 detectors and accuracy of the corresponding Monte Carlo predictions were tested in various setups at SLAC involving pulsed high-energy electron beams (up to 14.5 GeV, thus leading also to intense photon and neutron fields) at ESTB facility, and low-energy photons from a <sup>137</sup>Cs, 30 Ci source at the Radiation Calibration Facility (RCF).

Tests allowed identifying early bugs in the physics implementation, as well as hardware weaknesses (current leaks). After addressing all those, readings and predictions generally agreed within 20 %, sometimes even within a few percent, and did not show any intensity-driven bias across the range of measurements, which spanned five orders of magnitude average current, starting at a few pA. Another conclusion was that the RCF irradiation well was also an adequate facility to calibrate B1 detectors.

## ČERENKOV FIBER DETECTORS

### Physics Implementation of Čerenkov Fibers

Charged particles moving through a dielectric medium -like the silica of fibers- at a speed greater than the phase velocity of light generate so-called Čerenkov photons, which are emitted at a characteristic polar angle

\* This work was supported by Department of Energy contract DE-AC02-76SF00515

<sup>†</sup> msantana@slac.stanford.edu

$\theta_c = \arccos((\eta_r \cdot \beta)^{-1}) \approx 46^\circ$ , where  $\eta_r$  is the refraction index in the fiber ( $\eta_r \approx 1.457$ ), and  $\beta$  the relativistic factor ( $\beta \rightarrow 1$ ). As for the polar angle ( $\phi$ ), it is uniformly sampled within  $2\pi$ .

Assuming the fiber is not dispersive, i.e. its refraction index is nearly independent of photon frequency within the range of detectable Čerenkov frequencies, the production rate of Čerenkov photons ( $dncpdw$ ) per band width ( $d\omega$ ) and length of fiber crossed by high-energy charged particles ( $L_f$ ) is approximately equal to:

$$dncpdw = \frac{\alpha_{fs}}{c} \cdot \sin^2(\theta_c) \cdot ch^2 \cdot L_f \quad (1)$$

Where:

- $\alpha_{fs}$  is the fine structure constant ( $\approx 1/137$ )
- $ch$  is the charge of the particle

$L_f$  is determined by computing each track length of charged particles (actually only electrons contribute significantly) through the fiber and multiplying by the other factors in Eq.1. Čerenkov photons are started randomly along each track with the directing angles  $\{\theta_c, \phi\}$ . Each photon is then tracked to its first interception of the core/cladding interface, where the angle with respect to the normal is measured (via scalar product) to determine if the photon is sufficiently glancing, i.e. within  $8.678^\circ$  of the tangent plane, to be captured within the fiber for transportation to the photomultiplier.

Since the diameter of the core of LCLS-II fibers is small ( $\varnothing_F = 600 \mu\text{m}$ ), likelihood for production of Čerenkov that will ultimately be captured is low, thus the implementation scheme above had to include variance reduction techniques. First, the fiber axis is forced to be at one of the central planes of the voxel that the particle is crossing, and within a band no farther than some radii (default=5) from the crossing point. Then, the fiber transverse position within the band is resampled  $itn$  times until the particle hits the core. The final Čerenkov statistical weight is corrected by the number of trials ( $\times itn^{-1}$ ), and by the ratio between the cross section area of the band (band height  $\times \varnothing_F$ ) and the cross section of the scoring voxel. This ratio can be proven to be proportional to the *fluence* and to the normalized *transverse direction* of the charged particle. Thus, the fiber response model was implemented in the same fluence weighting user sub-routine “fluscw.f” used for B1 response.

Additionally, not just one, but  $n=10$  (default) Čerenkov of statistical weight  $1/n$  are generated per event, each with different polar angles. If any of those photons is successfully captured, more (default = 4) are generated within the vicinity of the successful  $\phi$  (and a further adjustment to the statistical weights is applied).

Other implemented effects include corrections for the finite range of electrons in the fiber (using the continuous slowing down approximation), accounting also for path spent in the outer (thicker) cladding. Likewise, production of

Čerenkov by photons through intermediate electrons generated at the fiber cladding or core may also be computed. The model allows filtering captured Čerenkov according to which PMT (up/downstream) they go to, and their intensity (i.e. statistical weight) can be reduced according to absorption and/or attenuation effects occurring along those paths.

To obtain the PMT signal as pC per simulated particle, the final count must be multiplied by the characteristics of the fiber/PMT, i.e. the quantum efficiency (e.g. 0.3), the amplification (e.g.  $1 \times 10^6$ ) and the filtered band-width (e.g.  $d\omega \approx 2E14 \text{ s}^{-1}$ ).

### Fiber Simulations vs. Measurements

Simulations of fiber response to irradiation of thick targets correctly reproduced the Čerenkov production peak at  $\approx 45^\circ$  from the beam axis, while the absolute reading was predicted within approximately a factor of 2. The code also anticipated an increase of readings (for same high energy  $e^-$  beams) for thinner targets, although absolute values overestimated the response by factors 5 to 7. In future revisions it may be worth exploring whether absorption of shallow angle electrons on the cladding of the fibers is sufficiently represented.

## APPLICATIONS AND CONCLUSIONS

Here we present a brief subset of the guidelines found for the placement of solid state detectors in high energy (4-20 GeV) electron accelerators, based on parametric FLUKA simulations with the scoring routine described before.

### Monte Carlo Simulations for Diamond Detectors

Figure 1 Flair [5] rendering shows the ratio of a B1 signal to the equivalent dose rate around a cylindrical thick copper target of  $15 X_0$  (21 cm) length and 1 Mo radius (1.2 cm). The ratio ranges from 1 to 12 pA/(mrem/h), varying strongly as a function of  $\theta$ . If the radius of the target is *doubled*, the ratio pA/mrem/h at  $\theta = 90^\circ$  is approximately reduced by the *same factor*. Iso-curves at 20 and 1000 pA/W were also drawn. Considering a lower detection limit (over noise) of about 100 pA, we conclude that B1 can detect losses on stoppers no lower than  $\approx 100 \text{ mW}$ , i.e. they cannot resolve dose rates below a few rem/h ( $\rightarrow$  inside detectors only).

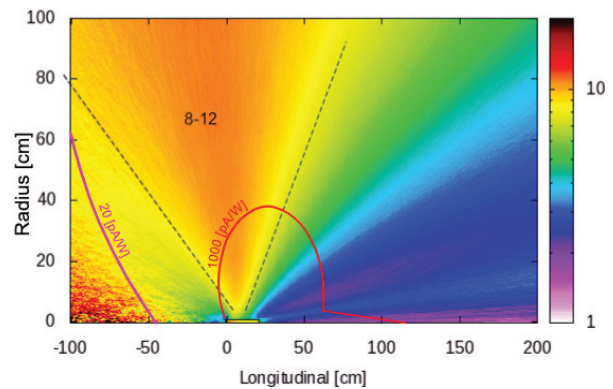


Figure 1: Expected *diamond signal to equivalent dose rate* ratio pA/(mrem/h) for 4 GeV  $e^-$  on a  $15 X_0$ , 1 Mo Cu target.

The response map is significantly different for thin and medium targets, such as the shielding masks that are installed along the beam-lines to intercept mis-steered beams and set beam shut-off signals on adjacent detectors. Simulations show that the response of B1 detectors is rather flat with beam energy and independent on  $z$  from 2 to 40 m downstream of the targets. Moreover, the response is insensitive to the offset of the mis-steered beam, as long as the detectors are at a minimum distance  $d \geq 150$  cm from the beam-axis. Thus, in LCLS-II a single B1 diamond can guard several upstream shield plates from either of the two parallel beam-lines (SXR and HXR), as explained in Fig. 2. Those detectors will not be sufficiently sensitive to sense losses on thick targets (e.g. QT41 magnet), since, as shown before, response falls off quickly moving away from such targets.

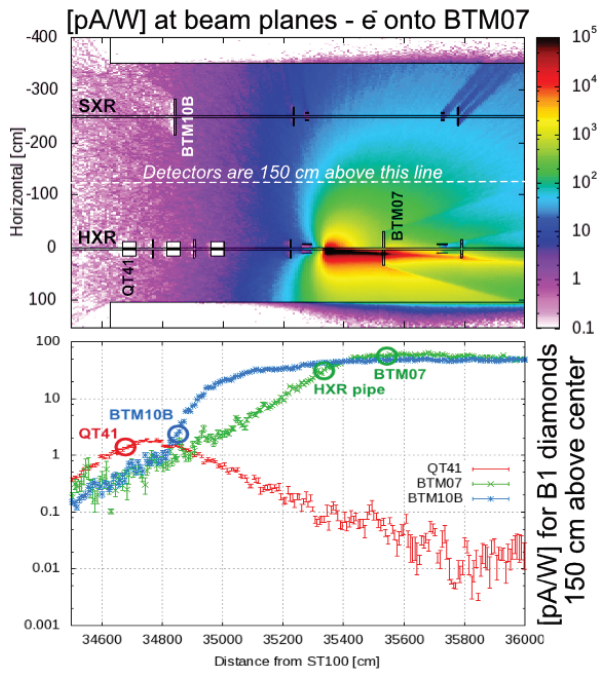


Figure 2: Expected signal pA/W for 4GeV  $e^-$  beams on (top) the 7.5 cm-thick BTM07 iron mask (signal at beam-planes), and (bottom) for this and other beam targets with B1 detectors 150 cm above the center of the tunnel.

Monte Carlo Simulations for Čerenkov Fibers

Simulations confirmed that most of the signal in a fiber is generated short down-beam of the target, i.e. 90% is integrated within the 20 m from thick targets and within 50 m from beam mis-steering on a pipe. Upstream contributions are minimal. As for the impact of the transverse distance ( $d$ ) of the fiber to the beam-line, Fig. 3 shows how the signal falls off relatively softly, as  $d^{-0.79 \pm 0.02}$ . Two additional important conclusions can be made:

- Signals from thinner targets are substantially higher ( $\times 10 - 40$ ) than from thick targets since for the latter escaping electron fluence is much lower.

- Scattered electrons and subsequent fiber signals are quickly shielded. The gap between thin and thick target induced signals is significantly reduced behind thick shielding (as inside of BTH walls).

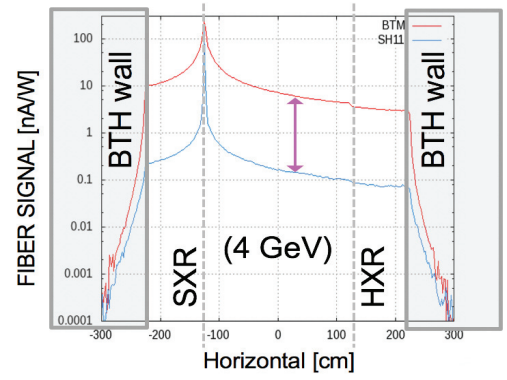


Figure 3:  $z$ -integrated fiber signal nA/W as a function of transverse distance to losses at SXR beam-line on BTH=mask or SH11=thick target.

Finally, simulations for field emission radiation fields [6] on LCLS-II linac, suggest only very high captured currents per cryomodule (e.g.  $\geq 100$  nA<sub>CM</sub>) will be readily detectable by fibers, where noise level at the PMT is a few nA.

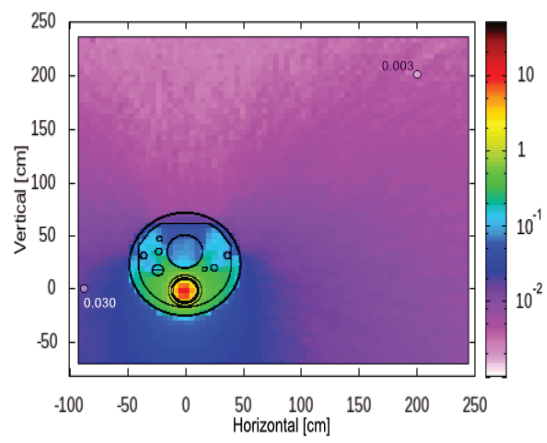


Figure 4:  $z$ -integrated fiber signal per field-emission captured current [ $nA_{PMT}/nA_{CM}$ ] as a function of the transverse position of the fiber.

REFERENCES

[1] A. S. Fisher, C. Field, L. Nicolas, "Evaluating beam-loss detectors for LCLS-2", *SLAC-PUB-16812*.  
 [2] T. T. Böhlen et al., "The FLUKA Code: Developments and Challenges for High Energy and Medical Applications", *Nuclear Data Sheets 120*, 211-214 (2014).

- [3] A. Ferrari, P. R. Sala, A. Fassò, and J. Ranft, “FLUKA: a multi-particle transport code”, CERN, Geneva, Switzerland, Rep. CERN-2005-10, 2005, INFN/TC\_05/11, SLAC-R-773.
- [4] S. Agostinelli *et al.*, “GEANT4 – A Simulation Toolkit”, *Nucl. Inst. and Methods in Physics Research Section A*, Volume 506, Issue 3, 1 July 2003, Pages 250-303.
- [5] V. Vlachoudis, “FLAIR: A powerful but user friendly graphical interface for FLUKA”, in *Proc. Int. Conf. on Mathematics, Computational Methods & Reactor Physics (M&C 2009)*, Saratoga Springs, New York, 2009.
- [6] M. Santana, L. Ge, Z. Li, C. Xu, C. Adolphsen, M. Ross, and M. Carrasco, “Studies of Radiation Fields of LCLS-II Super Conducting Radio Frequency Cavities”, *International Journal of Modern Physics: Conference Series*, Vol.44(2016) 1660209.